Aerosol Science and Engineering (2021) 5:344–356
https://doi.org/10.1007/s41810-021-00108-3

ORIGINAL PAPER

Detailed Physicochemical Characterization of the Ambient Fine and Ultrafine Particulate Mixture at a Construction Site

Firdevs Ilçi[1] · Mengfan Li[1] · Jeremy Gernand[1]

Received: 9 January 2020 / Revised: 26 May 2021 / Accepted: 2 June 2021 / Published online: 5 July 2021

Abstract

This paper presents a detailed characterization of the size and shape distributions, and chemical compositions of ambient fine and ultrafine particles collected at the site of a building demolition and construction project at the Pennsylvania State University. Particle samples were collected with a nine-stage cascade impactor, characterized via transmission electron microscopy and energy dispersive spectroscopy for elemental compositions, and images analyzed for morphological features. 89.3% of the particles collected by count were ultrafine particles or aggregates of ultrafine particles that disaggregated during the collection process. The mean particulate matter mass and count concentrations were 167.2 μg/m^3 and 16,232 particles/cm^3, respectively. 72.2% of the particles by count were morphologically circular on two-dimensional images and 74.0% of the particles by count had an aspect ratio of between 1:1 and 2:1. The five most prevalent elements found in the samples were carbon, oxygen, silicon, sulfur, and calcium, with corresponding mass fractions of 40.8%, 26.4%, 7.6%, 5.1%, and 4.7%. Based on the current regulatory occupational exposure limits, the particulate matter at the construction site was within permissible concentrations. These results enable a comparison of a real-world particulate exposure environment to hazard levels determined through single-particle-type exposure studies.

Keywords Ultrafine · Characterization · Particulate matter · Mixture · Exposure

1 Introduction

Particulate matter (PM) is a complex mixture of small particles and liquid droplets and is ubiquitous in environment. There is a growing interest in characterizing human exposures to particles with an aerodynamic diameter of less than 100 nm, known as ultrafine particles or UFPs when occurring in the ambient atmosphere whether anthropogenic or naturally occurring, or as nanoparticles when specifically manufactured or engineered. There is also a greater awareness of the need to understand the health, safety, and environmental impacts of UFPs (Yang et al. 2011). Various properties of engineered nanoparticles have led to their increasing production and use, resulting in increasing number of workers exposed to them (Scalf and West 2006).

Thus, the evaluation of the potential occupational health risks of the exposure to UFPs and nanoparticles is essential to ensure their safe manufacturing and handling in workplaces. Since the atmosphere in traditional workplaces is likely to already contain inadvertently created analogues of engineered nanoparticles, these sites present valuable investigation opportunities for understanding the long-term impacts of these exposures if the degree of similarity can be clarified.

1.1 Sources of Ultrafine Particles

Products of combustion processes and secondary atmospheric transformations appear to be the major sources for ambient UFPs, and relevant contributions of these sources to ambient UFPs concentrations might change with location, season, and time-of-day (Health Effect Institute 2013). Specifically, motor vehicle exhaust is a major contributor to UFP concentrations in proximity to major roads in urban areas (Asadi and Hassan 2014). Additionally, UFPs are also commonly associated with other combustion-related processes,

✉ Jeremy Gernand
jmgernand@psu.edu

[1] John and Willie Leone Family Department of Energy and Mineral Engineering, The Pennsylvania State University, University Park, PA, USA

including the burning of biomass and the combustion of fossil fuels (Health Effect Institute 2013).

Different operations or facilities feature PM of different chemical compositions and sizes. Within a stainless-steel production plant, the sintering plant featured particles with an aerodynamic diameter larger than 1 μm (or 1000 nm) containing Cr, Fe, Al, and Mg, whereas the hot rolling mill featured particles with the aerodynamic diameter between 10 and 20 nm mainly containing Fe, Cr, and Ni (Järvelä et al. 2016). Diesel engines of all types continue to be a concern for particles emission, and a study at a port of Montréal, Canada, showed that 79% of all sampled ambient particles by mass were smaller than 1 μm (Debia et al. 2016). Another study focusing on road paving emissions found that 80% of the ambient particles by mass were finer than 1 μm in laboratory conditions (Weiss et al. 2018).

The particles emitted from a construction site or an industrial area can be characteristic. Local average PM concentration tended to be greater at these sites than that at urban sites; chemically, NO_3^-, Cl^-, SO_4^{2-}, Na^+, and NH_4^+ made up the majority of detected water-soluble ions from the PM samples, and Ca, Fe, Al, and Zn were the most common metal elements found in PM samples (Hama et al. 2018). A study in central Italy showed that aluminum silicates and calcium-rich particles were prevalent in the coastal industrial site, largely due to construction activity; the aluminum silicates featured a wide range of morphologies from a minimum circularity of 0.21 to a maximum of 0.89, and the calcium-rich particles comprised of $CaCO_3$ and CaO probably originated by the processes of construction, demolition, and cement factories, who morphologically moved away from spherical shape with an average circularity of 0.68 (Campos-Ramos et al. 2009; Genga et al. 2018).

Both short-term and long-term exposures to ambient PM result in increased mortality and hospitalization due to cardiovascular and respiratory diseases (Health Effect Institute 2013). A major route of the exposure to UFPs is through the respiratory system and they have been known to trigger cardiovascular diseases-related mortality and to induce respiratory diseases, such as chronic obstructive pulmonary disease (COPD) and pulmonary fibrosis (Du et al. 2016; Falcon-Rodriguez et al. 2016). The different parts of the respiratory system subject to the preliminary effects of exposure and the amount of time that UFPs take to move into the lungs are affected by several factors, such as size, shape, and density of PM (Suhaimi and Jalaludin 2015). Other than cardiovascular and respiratory symptoms, the exposure can also lead to neurodevelopmental disorders during the human third trimester equivalent, such as autism spectrum disorder and schizophrenia, and increase the odds for pediatric multiple sclerosis (Allen et al. 2017; Lavery et al. 2018).

Animal studies have revealed that UFPs could be inhaled more deeply into the lungs and make exposed population more easily develop airway inflammation than could larger particles, because the former have a higher specific surface area, through which superficial toxic chemicals have a greater chance of being adsorbed by human (Zhang et al. 2010).

1.2 Motivation and Objective

Previous studies have not yet undertaken a simultaneous characterization of either size or shape and chemical composition of fine PM and UFPs mixtures. Also, it is still unknown if particles collected in contemporary work sites can be characterized to a similar degree as those examined in well-controlled experiments in laboratories. This sort of process will be necessary to fully understand PM exposure risks in the future and bound our expectations regarding occupational exposures to engineered nanomaterials.

Regulators around the world are considering new exposure limits for nano-particulates in light of the research being produced on the increased toxicity of these UFPs whether engineered or naturally occurring, but it is yet unclear how such limits will be defined and enforced. The construction industry is in need of detailed characterization data that can help it understand the extent of existing risks as well as the potential impact of future regulations on exposures to these small particles.

This research study aims to measure and characterize size distributions, number and mass concentrations, shapes, and chemical compositions of PM and UFPs mixture, and to show that non-intentionally created nanoparticles exist in non-trivial quantities, and evaluate the extent to which an occupational health risk may be present, with aerosol area samples collected from a construction site.

2 Methods

2.1 Sample Collection

The collection site was adjacent to the active area of the Steidle Building renovation project at the Pennsylvania State University, located in a rural college town in Pennsylvania. There is only limited traffic in the vicinity to the construction site with the road adjacent to the building only carrying internal campus traffic and no through traffic. The nearest road with general traffic to the building site is located more than 300 m away. The demolition and construction project began in July 2014 and completed in July 2016 (Duclos 2015; Penn State Office of the Physical Plan 2018). Sample collecting took place on four separate occasions between September 2014 and September 2015. Sample collection was accomplished on calm sunny days, since previous experience suggested that precipitation or fog could adversely affect

Table 1 Sampling temporal and weather information

Date	Sample time start	Sample volume (L)	Temp. (°C)	Relative humidity (%)	Weather condition
12 September 2014	3:00 pm	120	21	61	Sunny
16 October 2014	2:00 pm	120	17	33	Sunny
22 March 2015	2:30 pm	240	8	74	Sunny
18 September 2015	11:30 am	240	16	75	Sunny

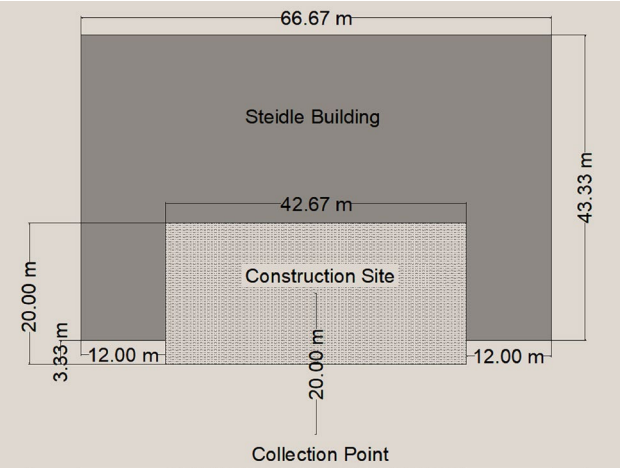

Fig. 1 Ambient particles samples collection setup

the persistence of the target particles; for example, windy weather could have an undesired impact on the concentrations and the kinds of PM (Kittelson et al. 2004; Drewnick, 2008; Bzdek et al. 2012). Temporal and weather detail about samplings can be found in Table 1. Area PM sampling with the impactor occurred approximately 20 m away from the center of the site and 1.5 m above the ground, as shown in Fig. 1. Since renovating the south façade of the Steidle Building was part of the project, the site remained an open space for a majority of construction hours.

This sampling location was selected to ensure equipment stability and support the demonstration of the method described in the following section to characterize complex mixtures of particulate matter. This area sample has some relevance to the safety of the general public in the vicinity of these worksites but is not ideal for making inferences about the safety of any construction workers by their specific occupation; though workers predominately outdoors would experience a very similar environment to that analyzed here.

2.2 Equipment

A PIXE nine-stage cascade impactor (PIXE International Corp., Tallahassee, FL) was used to collect PM samples from the demolition and construction site. With the PIXE cascade impactor, PM can be categorized into ten aerodynamic

Table 2 GAST DOA vacuum pump calibration

Designed flow rate (L/min)	Measured flow rate (L/min)
1.000	1.012
1.000	1.023
1.000	1.019

diameter intervals or stages: > 16 µm, 16–8 µm, 8–4 µm, 4–2 µm, 2–1 µm, 1.0–0.5 µm, 0.5–0.25 µm, 0.25–0.12 µm, 0.12–0.06 µm, and < 0.06 µm. These ten intervals provide adequate resolution to characterize aerosols in the region of interest. The impactor is molded of electrically conductive polymer with O-ring seals and is designed for a pumping rate of 1.0 L/min. A GAST DOA-V502-JH model vacuum pump (Gast Manufacturing, Inc., Benton Harbor, MI) was connected to the impactor via a plastic hose with an internal diameter of 0.48 cm and a length of 2.5 m to minimize the likelihood of capturing particles from the pump exhaust.

Bios Defender 510-M Calibrator with flow calibrator (Mesa Labs Inc, Butler, NJ) was used to calibrate the vacuum pump and cascade impactor assembly. A flow-metering device, Dwyer RMB-50D-SSV (Dwyer Instruments Inc., Michigan City, IN) was used to monitor the air flow rate maintained at 1 L/min. The calibration data can be found in Table 2.

A Philips 420 Tungsten-based 120 kV transmission electron microscopy (TEM) with an energy dispersive spectroscopy (EDS) via DeskTop Spectrum Analyzer (DTSA) program (Philips Inc., San Francisco, CA) and an FEI Tecnai G2 Spirit BioTwin 20–120 kV TEM with EDS via EDAX program (FEI Inc., Hillsboro, OR) were used to establish complete particles size distributions. TEMs are now one of the best methods to obtain mineral fiber concentrations, size measurements, and specific identification in almost all environmental situations. The EDS was used to analyze the chemical composition of particles by matching the spectral peaks for each chemical element present.

Carbon-coated copper grids with a diameter of 3 mm for a TEM (200 Mesh, Cu PK/100) by SPI (SPI Supplies, Inc., West Chester, PA) were fixed using Kapton adhesive onto the polytetrafluoroethylene (PFTE) membranes of each stage of the cascade impactor.

2.3 Blank Analysis

A blank analysis was conducted to show that the grids did not collect any particle or contaminants from transport or handling or removal from the relevant devices. No mass differences were observed on the grids of the cascade impactor (filter size from 4–2 μm to < 0.06 μm) before and after placing the impactor at the same construction site without operating; gravimetric measurement data can be found in Table 3. Additionally, TEM images further confirm that there existed no particles on the grids at different magnifications, as shown in Fig. 2.

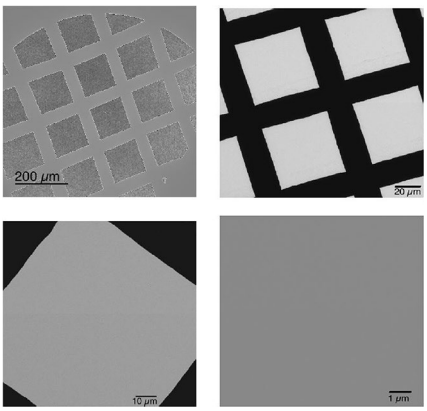

Fig. 2 Empty grids images with four different magnifications from TEM analysis. No particle was observed in the process of media loading or unloading

2.4 Sample Analysis

After all the grids were confirmed blank via gravimetric measurements and TEM analysis, they were placed on the PFTE membranes of the impactor stages to collect particles. A minimum of ten non-overlapping images were captured for each grid with the TEM. Images were selected according to two different criteria: (1) the appearance of multiple particles together in the image for evaluating size and shape distributions of particles on grids; and (2) the appearance of one individual particle in the field of view for chemical analysis via the EDS. After taking the pictures of particle samples by the TEM, the EDS was used to analyze elemental compositions of ten randomly selected particles present in the TEM image individually, one at a time.

Since the TEM grids are made of carbon-coated copper, we lost the ability to distinguish copper and carbon in our sampled particles. For this reason, when imaging a particle made entirely of copper or carbon, the EDS results will show a similar pattern of peaks as to our blank analysis described in the above section. Since copper particles are anticipated to be rare, and carbon particles (from combustion sources) common, we will assume that EDS-analyzed particles showing peaks identical to the background will be assumed to be made of carbon.

Following the sample collection activity, the TEM grids were again measured gravimetrically by the Cubis-Sartorius MSA2.7S-000-DF microbalance. In each case, prior to the mass measurement, the grids were stationed in a climate controlled room within a glass container containing silica gel desiccant for 24 h. Each grid was measured three times before and after the sample collection activity. The mean of these three measurements was then recorded with the difference determining the collected mass within that impactor stage.

2.5 Data Processing

The software Image J (National Institute of Health, Bethesda, Maryland) was used to determine particles size, particles number concentrations, and particles density across the total collection area from the pictures captured by the TEM. Image J is a Java-based image-processing program, developed by the National Institutes of Health (NIH) (Image J 2001). Each sample picture obtained by the TEM was characterized by Image J to determine the diameter of particles with the formula:

$$d = \sqrt{\frac{4A}{\pi}}, \tag{1}$$

where d is the diameter and A is the area of the particle. Once an image of a particle was digitized and the edges of each particle were defined, shape factor measurements

Table 3 Gravimetric measurement of grids by Cubis-Sartorius MSA2.7S-000-DF

Grid stage (μm)	Mass before blank (mg)				Mass after blank (mg)			
	Trial 1	Trial 2	Trial 3	Mean	Trial 1	Trial 2	Trial 3	Mean
4–2	0.5285	0.5292	0.5290	0.5289	0.5289	0.5291	0.5290	0.5290
2–1	0.5389	0.5395	0.5396	0.5393	0.5395	0.5388	0.5387	0.5390
1–0.5	0.5119	0.5125	0.5122	0.5122	0.5122	0.5120	0.5121	0.5121
0.5–0.25	0.5810	0.5816	0.5816	0.5814	0.5815	0.5812	0.5815	0.5814
0.25–0.25	0.5478	0.5487	0.5484	0.5483	0.5481	0.5482	0.5486	0.5483
0.12–0.06	0.5757	0.5764	0.5762	0.5761	0.5761	0.5763	0.5759	0.5761
< 0.06	0.4967	0.4974	0.4975	0.4972	0.4970	0.4972	0.4974	0.4972

could then be made (Olson 2011). Quantities of aspect ratio and circularity would be calculated to further characterize the particles.

Aspect ratio describes the proportional relationship between width in the major axis and height in the minor axis. It was calculated based on the formula below:

$$\mathrm{AR} = \frac{\text{Width (Major Axis)}}{\text{Height (Minor Axis)}} \quad . \tag{2}$$

Therefore, aspect ratio by definition has a minimum of 1.0:1.

Circularity is defined as the degree, to which the particle is similar to a circle. Its value is bounded between 0 and 1: a circularity of 1 indicates a perfect circle, whereas a circularity of 0 indicates an elongated polygon. It was calculated based on the formula below:

$$C = 4\pi \frac{A}{P^2} \quad , \tag{3}$$

where A is the area of the particle, and P is the perimeter of the particle.

It should be noted that aforementioned described image analysis techniques proceed to infer properties of three-dimensional particles from two-dimensional images, suggesting that these techniques are unable to distinguish between spheres and flats, circular disks as well as other similar two-dimensional projections of three-dimensional particles.

3 Results

3.1 Particle Size and Size Distribution

For the collected particles, the maximum particle diameter as measured via the image analysis was 10.5 µm (or 10,500 nm), the minimum particle diameter measured was 0.00099 µm (0.99 nm), the mean diameter was 0.046 µm (or 46 nm), and the mode diameter was 0.0044 µm (or 4.4 nm). This size interval of from 0.99 nm to 10.5 µm included ultrafine, fine, and coarse particles. Figure 3 indicates the particle size distribution by count for the entire ambient particle mixture. 99.5% of the particles sampled by count were finer than 1 µm and 89.3% of them could be classified as UFPs (i.e. < 0.1 µm). Since almost all particles collected had a diameter of less than 4 µm, they could be classified as respirable particles by the American Conference of Governmental Industrial Hygienist (ACGIH) (2005).

3.2 Mass and Number Concentrations

The mean PM mass concentration was measured as 167.2 µg/m^3 with the greatest mass fraction corresponding

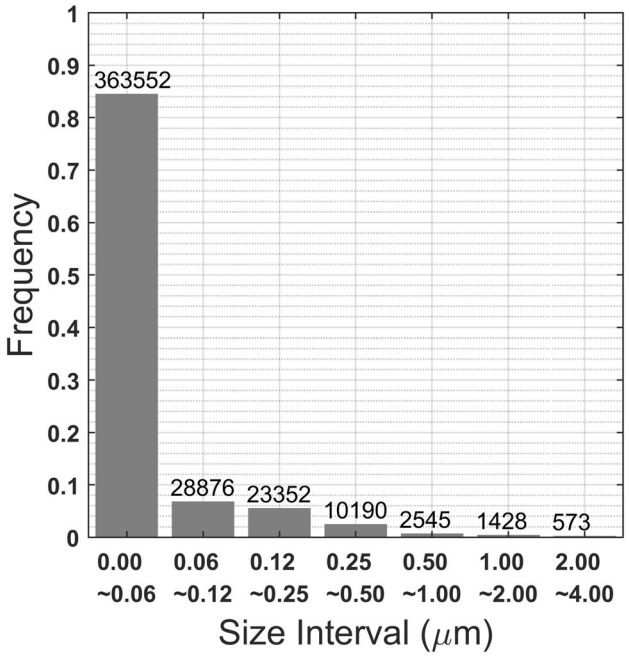

Fig. 3 Overall particle size distribution by count from all samples. Numbers above each bar refer to number of sampled particles in each interval. 99.5% and 89.3% of particles by count were finer than 1.0 µm and 0.1 µm, respectively

to a concentration of 67.7 µg/m^3 within the coarsest interval between 2 and 4 µm, shown in Fig. 4, as the coarser particles are expected to contain greater mass. As of 2018, the Occupational Safety and Health Administration (OSHA) has an 8-h time weighted averaged (TWA) permissible exposure limit (PEL) for particulates not otherwise regulated (PNOR) at 10,000 µg/m^3 (10 mg/m^3) for total dust and 5000 µg/m^3 (5 mg/m^3) for respirable fraction (United States Department of Labor 2018). According to the latest regulatory criteria, the PM sampled at the construction site in this study did not pose a significant threat to occupational health.

The mean PM number concentration was 16,232 particles/cm^3. The lowest number concentrations of 135 particles/cm^3 by particle size category was found with the size range of < 0.06 µm, and the highest concentration by size category, 9463 particles/cm^3, was found within the size range of 0.5–0.25 µm, as shown in Fig. 5.

3.3 Shape Analysis

Among all 430,553 particles with their images obtained, 72.2% by count had a circularity value of between 0.9 and 1, with a mean of 0.88 and a standard deviation of 0.22, as shown in Fig. 6. 74.0% by count had an aspect ratio of between 1:1 and 2:1, with a mean of 1.48:1 and a standard deviation of 0.75. The correlation coefficient between

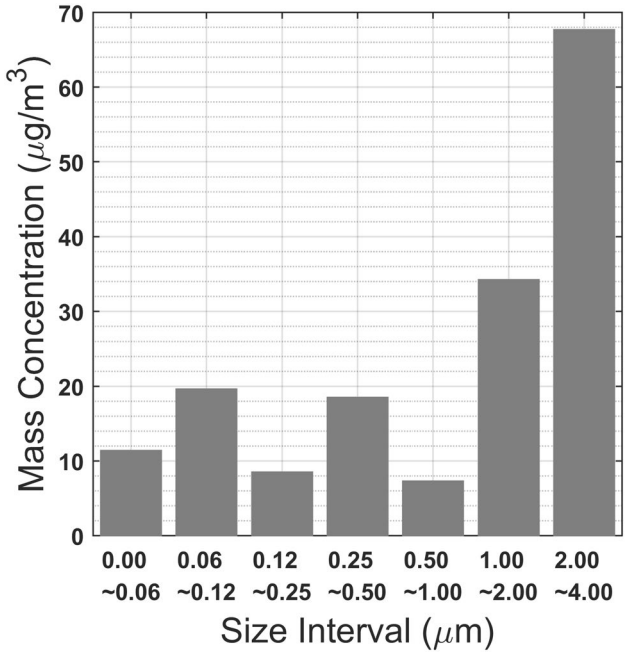

Fig. 4 Particle mass concentration for all samples. The mean mass concentration was measured at 167.2 μg/m^3. Particles with a dimeter greater than 1 μm constituted the majority of mass concentration

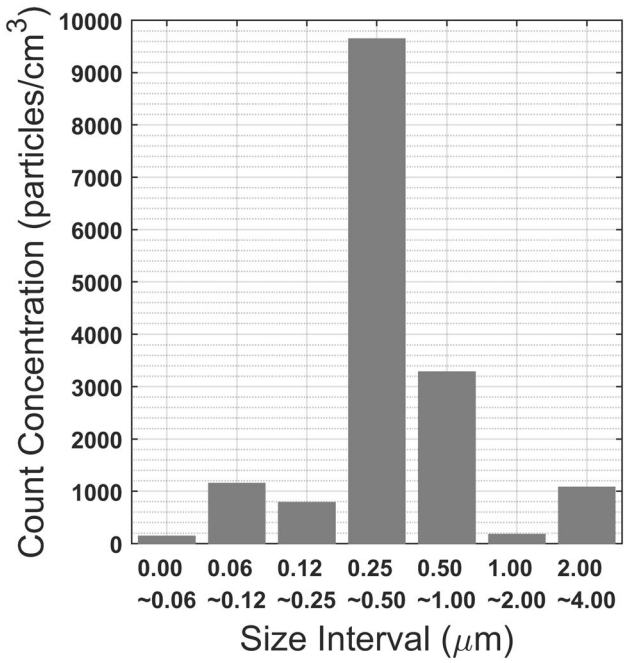

Fig. 5 Particle count concentration according to size intervals. The mean count concentration was measured at 16,200 particles/cm^3

circularity and aspect ratio was – 0.50, indicating a minor inverse correlation.

Results of circularity and aspect ratio were in agreement, as a particle with a circularity above 0.9 is morphologically close to a circle on a two-dimensional image, whose aspect ratio should not deviate significantly from 1:1.

3.4 Chemical Composition

The mass fraction of each individual element is independent of the chemical form of that element. Shown in Fig. 7 are the mass fraction distributions for non-trivial elements of entire samples from the EDS. C, O, Si, S, and Ca were the five most prevalent elements detected, with an overall mass fraction of 40.8%, 26.4%, 7.6%, 5.1%, and 4.7%, respectively, as shown in Fig. 8. The mass concentrations for individual elements were an inference, based on an overall mass concentration as 167.2 μg/m^3.

Both C and O made up at least 56.3% of the samples by mass in every size interval, the latter of which was presumably in the form of oxides, sulfates, and carbonate compounds. As mentioned in Sect. 2.4, carbon content is inferred from particles that do not show any unique peaks differing from the background of copper and carbon created by the TEM grids themselves. The presence of Si and Al was expected to come from building demolition activities, as they are major constituents of bricks and cement (Lioy et al. 2002; Azarmi et al. 2015). S was measured with the highest mass fraction of 17.9% in the interval between 0.5 and 1.0 μm; S, Mg, and Zn are considered common ingredients of exhaust emission from diesel engines, so transport trucks and demolition and renovation machinery at the site might contribute to their levels (Dorado et al. 2003; Thorpe and Harrison 2008). Co was detected with peak mass fractions of 8.5% and 8.7% in the respective intervals between 0.25 and 0.50 μm and between 2.0 and 4.0 μm, and its presence could be attributed to fugitive dust generated by demolition activities on site (Amato et al. 2009; Crilley et al. 2017).

Additional caution is needed to further infer the chemical composition of the sampled particles, as it is not possible through this analytical method to identify whether the work site atmosphere had metal oxides or metal carbonates in specific proportions.

3.5 Hazard Analysis

If C was present solely in the form of carbon black at the sampling site, its mass concentration would be estimated at 68.2 μg/m^3, as shown in Fig. 8. The current recommended TWA exposure limit for carbon black by the National Institute of Occupational Safety and Health (NIOSH) is 3500 μg/m^3, which is well above the mass concentration from the sample (United States Department of Labor 2018). One additional note is that carbon black would be considered a potential occupational carcinogen by NIOSH if polycyclic aromatic hydrocarbons (PAH) were together with carbon black, whereas the existence

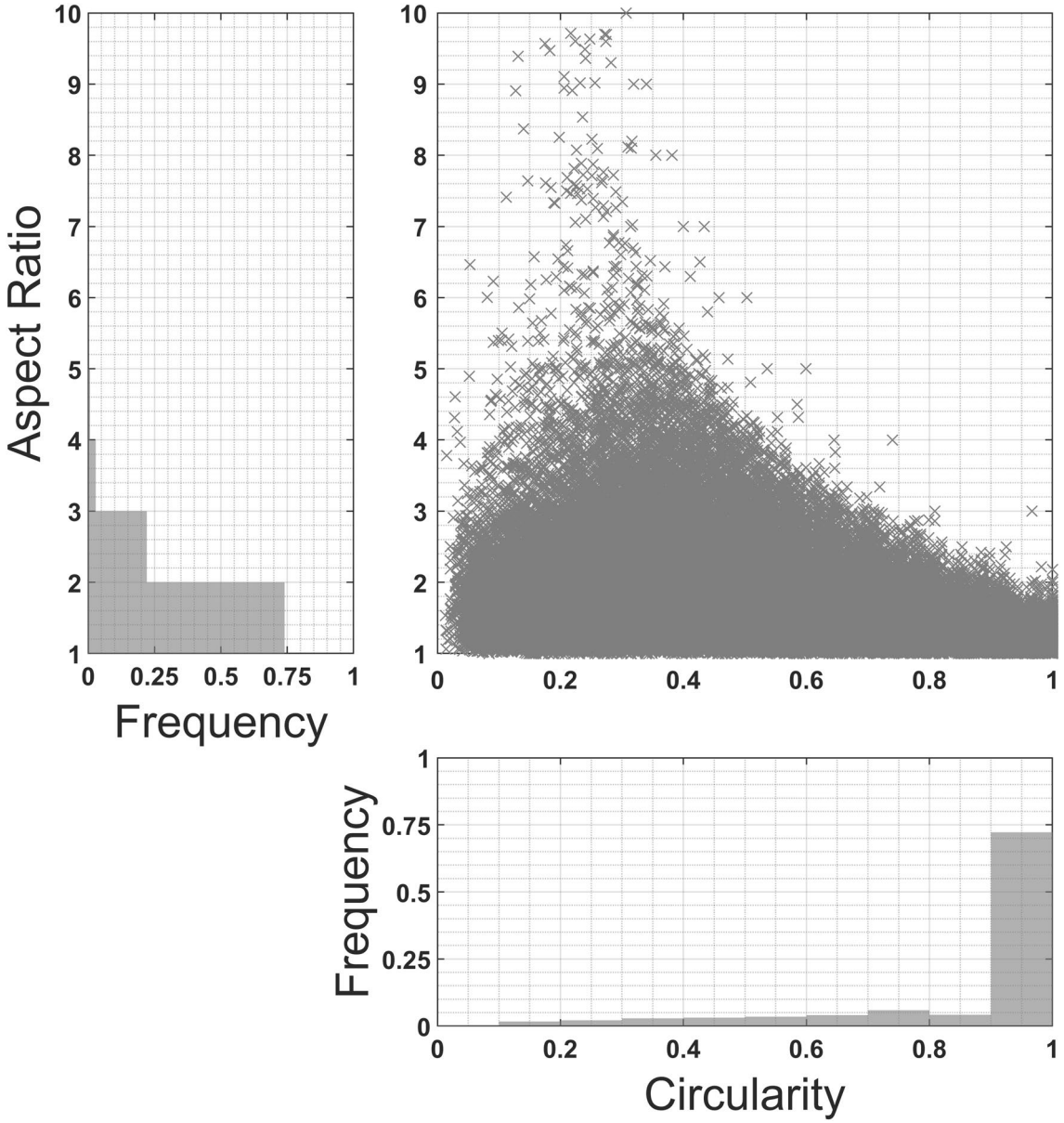

Fig. 6 Relationship between aspect ratio and circularity (displaying data from all 430,554 imaged particles). Particles in the upper left quadrant of the graph are rods or fibers, while particles in the lower left quadrant are predominately fractal in shape

of PAH was unknown based on results obtained from this study (United States Department of Labor 2018).

O had a mass fraction of 26.4%, and was likely in from of oxides and carbonate compounds, such as $CaCO_3$, Fe_2O_3, MgO, ZnO, and B_2O_3, which have TWA recommended exposure limits (RELs) of 5000 μg/m^3 (respirable fraction), 5000 μg/m^3, 10,000 μg/m^3, 5000 μg/m^3, and 10,000 μg/m^3, respectively (United States Department of Labor 2018). The total PM mass concentration of 167.2 μg/m^3 was lower than any of the individual TWA RELs. Hence, metal and non-metal oxides mass concentrations in this construction area presented a marginal hazard level for workers at the sampling location.

Si had a mass percentage of 7.6% and its estimated concentration was 12.7 μg/m^3, the latter of which was fraction of its TWA REL of 5000 μg/m^3 (United States Department of Labor 2018). For the last two prevalent elements found, S and Ca, their mass concentrations were estimated to be 8.46 μg/m^3 and 7.92 μg/m^3, respectively. The RELs as elemental bases could not be found for these two elements; however, their oxide compounds (SO_2 and CaO) are subject to the TWA RELs of 2 ppm (equivalent to 5230 μg/m^3 at

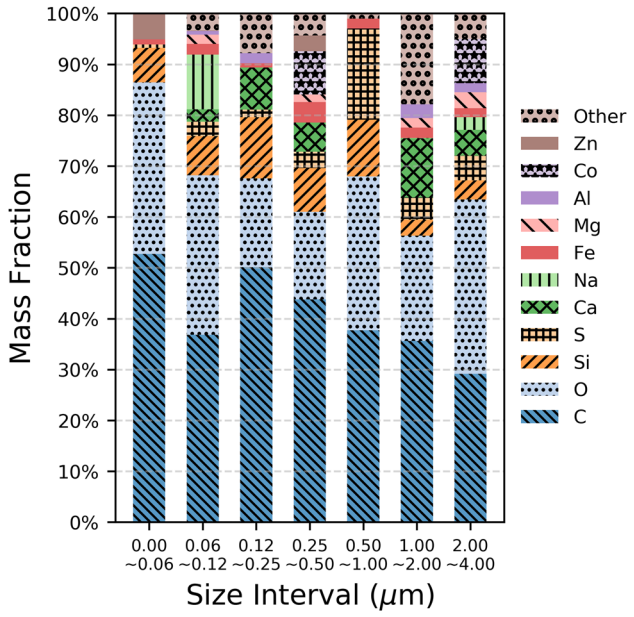

Fig. 7 Chemical elemental composition of particles according to size intervals. Carbon, oxygen, silicon, sulfur, and calcium were the five most prevalent elements found in all four sampling periods

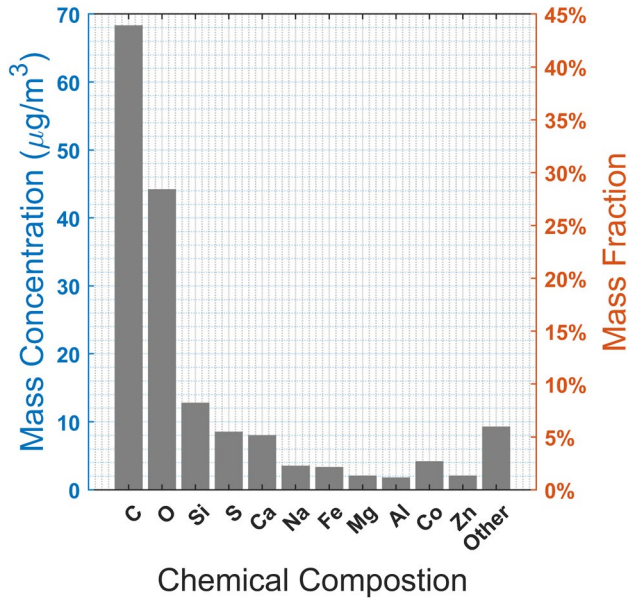

Fig. 8 Overall mass concentrations and mass fractions by chemical composition. The mass concentration was an estimation based on an overall mass concentration of samples at 167.2 μg/m^3

room temperature and atmospheric pressure) and 2000 μg/m^3, respectively (United States Department of Labor 2018). The mass concentrations for both elements were lower than their TWA RELs.

Regarding elements detected other than the five most prevalent ones (i.e., Na, Fe, Mg, Al, Co, Zn), and their mass fractions and estimated mass concentrations ranged from 1.0 to 2.5% and from 1.74 to 4.10 μg/m^3, respectively. None of these elements in any of the expected chemical forms exceeded the established standards or recommendations.

It should be noted here that chemical composition is being partially inferred from elemental data that is limited by the EDS to distinguish copper and carbon in the sampled particles from the carbon-coated copper grids used for collection. Chemical composition can vary significantly even keeping elemental composition the same, so the above described hazard analysis is speculative. Future work should confirm the chemical composition of the particulate samples.

3.6 Small Particles Disaggregating During Collection

During image analysis of the imaged particles, they accumulated on each stage of the cascade impactor frequently differed from the expected stage size range of the impactor stages. An example of this phenomenon is displayed in Fig. 9. This does not appear to be a result of the imprecise or probabilistic size cutoffs between states. UFPs tended to appear on all stages of the impactor, especially as the result of what appeared to be disaggregation that occurred during particle impact. Additionally, other UFPs tended to appear by themselves in a position that was not easily attributed to disaggregation. This occurred on collection media from each stage of the impactor. This observation may have implications for gravimetric analysis of fine and ultrafine particulates in the future at least with the specific equipment used here.

4 Discussion

4.1 Implications of PM Size Distribution

The existence or non-presence of specific activities at construction sites likely impacts the PM size distribution. During each sample collecting period for this study, the construction site was active. Compared to the PM size distribution of inactive demolition sites near Zhengzhou, China, by Jiang et al. (2018), roughly 50% and 90% of particles by count had a diameter of less than 0.1 μm and 1.0 μm, respectively, whereas this study witnessed 89.3% and 99.5% of particles with corresponding size intervals. Additionally, surrounding buildings might prevent particles from being dispersed and leaving the site, such as the construction site in this study, but the notes by Jiang et al. (2018) indicated that at least two of the seven demolition sites investigated were actually void of any nearby building, which would be considered open ground and six of the seven had debris covering the ground. Higher concentrations of smaller particles

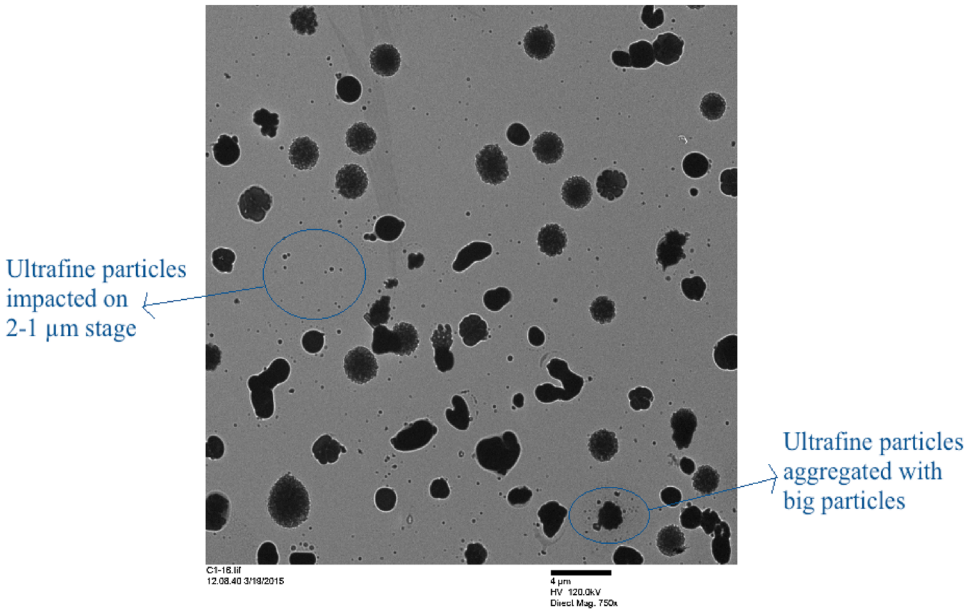

Fig. 9 Transmission electron micrograph displaying particles collected on the 1–2 µm stage of the cascade impactor. A combination of fine and ultrafine particles impacted on this stage possibly as a result of impact-caused disaggregation

during periods of greater activity at the site support the conclusion that these exposures will primarily be an occupational health concern other than an environmental public health concern.

The NIOSH REL for TiO_2 has recently been modified to account for particle size and now stands at 2.4 mg/m^3 for fine TiO_2 and 0.3 mg/m^3 for ultrafine TiO_2 (The National Institute for Occupational Safety and Health 2011). If future exposure limits are defined downwards for other fine and UFPs typically found at construction sites like gypsum ($CaSO_4{\cdot}2H_2O$) or silica (SiO_2), then further investigation will be critical to understand the specific activities and processes responsible for the increased production of these smaller particles.

4.2 Similarity to Other Occupational Environments (PM Mass and Number Concentrations)

In general, the overall mass and particle count concentrations from this study did not deviate significantly from those obtained from other studies focusing on outdoor construction or industrial activities, compared to a total PM mass concentration from 16 to 112 µg/m^3 with a mean of 47.5 µg/m^3 measured at a sea port of Montréal, Canada, reported by Debia et al. (2016) and that of between 60.5 and 379 µg/m^3 reported by Weiss et al. (2018) near the proximity of road paving activity for different mastic asphalt mixtures with different temperatures. On the contrary, indoor industrial activities could generate much higher PM mass concentrations: For instance, Azarmi et al. (2015) reported that room refurbishing activities could introduce a mean PM concentration ranging from 505 to 1593 µg/m^3; D'Arcy et al. (2016) found that an automobile production facility could have a mean PM mass concentrations ranging from 58 µg/m^3 at paint ovens to 680 µg/m^3 at aluminum diecasting; Järvelä et al. (2016) found that a stainless steel production facility had a PM concentration of 2340 µg/m^3 during the stainless steel melting process; Fent et al. (2018) at a simulated indoor fire scenario obtained a respirable PM mass concentration ranging from 63,050 to 715,000 µg/m^3 with a mean of 484,000 µg/m^3. The absence of obstacles that otherwise would have prevented ventilation in the outdoor construction area could be the contributor to the difference in PM mass concentrations measured between the indoor and outdoor environments. So, the particular environment investigated here was not particularly unusual in aggregate terms on a mass basis, though the resolution of the PM size distribution was finer.

Similar to the PM mass concentrations, the PM number concentrations from this study and other outdoor studies also agreed: Debia et al. (2016) reported particle number concentrations ranging from 16,544 to 57,314 particles/cm^3 with a mean of 36,381 particles/cm^3 near the Montréal port. Nonetheless, the PM number concentrations measured in indoor activities were greater by at least one order of magnitude. D'Arcy et al. (2016) recorded mean PM count concentration ranging from 9200 particles/cm^3 at body shop welding to 380,000 particles/cm^3 at aluminum die casting; Fent et al. (2018) reported particle number concentration ranging from 102,700 to 2,970,000 particles/cm^3 with a mean of 1,580,000 particles/cm^3 during the active simulated residential fire, and Järvelä et al. (2016) reported mean particle number concentrations ranging from 57,500 particles/cm^3 at cold rolling mill to 662,000 particles/cm^3 at ferrochromium smelter. Therefore, the spatial confinement of activities is

rendered a major factor in an exceedingly high PM number concentration in the indoor activities.

4.3 Implications of PM Geometric Properties

To the knowledge of the authors, while there are many investigations of particle size distributions in both laboratory and ambient environments (Chrysikou and Samara 2009; Apple et al. 2010; Deshmukh et al. 2013), there are not many investigations of the particle shape distributions in ambient air environments (Ault et al. 2012, 2013). In fact, such investigations when they occur, tend to either be qualitative in nature, or aimed at differentiating a manufactured particle from more mundane particle sources (Ono-Ogasawara et al. 2009).

For the few cases, where shape distributions of ambient particles were reported, such as a study in a coastal industrial site of Central Italy by Genga et al (2018) showing that locally prevalent aluminum silicates and calcium-rich particles had equivalent circularities (the authors reported the values in roundness, which is the reciprocal of circularity) ranging from 0.21 to 0.92 with a mean of 0.60 and ranging from 0.16 to 0.94 with a mean of 0.68, respectively, there is evidence of variation from the environment studied here that should be of interest to future researchers. The difference can be attributed to the remoteness of this study's construction site to oceans, as erosion tending to make particles more spherical over time and the Italian site proved to have sea salts with a lower mean circularity of 0.48, indicating less erosion than were the particles at the construction site subject to (Genga et al. 2018).

Even in indoor environments with significant manufactured nanoparticle exposure, other particle sources will still remain a substantial portion of total exposure. Understanding the relationship between the total exposure to particles of certain shapes (especially rod- and fiber-like particles) should be of interest. Image analysis of ambient PM such as the one conducted here will likely be the best way of obtaining this shape distribution data for the near future, and it should be considered an important part of completely characterizing complex environmental mixtures.

4.4 Implications of PM Elemental Properties

A major limitation of these analytical methods is that chemical composition can only be inferred but not directly determined. In cases where there are major differences in the potential toxicities of chemical compounds from the possibilities defined by the elemental analysis, a companion study should evaluate the prevalence of each of these potential compounds. This type of analysis would require the collection of greater quantities of particles, and the associations between the sizes and shapes of particles and their chemical compositions would not be as specific.

A comparison of chemical compositions was made to four other studies also focusing on demolition or construction sites in different geographical regions, listed in Table 4. The study by Jiang et al. (2018) explored inactive demolition

Table 4 Chemical compositions comparison to other studies also focusing on demolition and construction sites in different geographical regions

	This study	Jiang et al. (2018)	Azarmi and Kumar (2016)	Ramirez et al. (2019)	Amato et al. (2009)
Location	University Park, US	Zhengzhou, China	Heyward Heath, UK	Bogota, Colombia	Barcelona, Spain
Site type	Demolition and construction	Demolition	Demolition	Industrial	Demolition and construction
C	40.8%	11.7% ± 8.8%[a]	16.7%	14.6% ± 7.2%[b]	10.8%[c]
O	26.4%	n/a	48.5%	n/a	n/a
Si	7.6%	n/a	17.8%	25.3% ± 13.4%	9.6%[d]
S	5.1%	0.4% ± 0.4%[e]	2.3%	0.4% ± 0.2%	0.4%
Ca	4.7%	1.1% ± 0.5%	n/a	6.0% ± 2.6%	15.4%
Na	2.1%	0.1% ± 0.1%	2.5%	0.7% ± 0.1%	0.3%
Fe	2.0%	1.7% ± 0.5%	n/a	4.7% ± 2.0%	3.8%
Mg	1.2%	0.2% ± 0.6%	1.4%	0.6% ± 0.3%	1.3%
Al	1.0%	3.7% ± 0.6%	5.1%	9.6% ± 5.1%	4.5%[f]
Co	2.5%	Trace	n/a	Trace	Trace
Zn	1.2%	0.4% ± 0.2%	n/a	Trace	Trace

[a]Elemental carbon 1.1% ± 1.2% and organic carbon 10.6% ± 7.6%

[b]Elemental carbon 0.25% ± 0.38% and organic carbon 14.3% ± 6.94%

[c]Elemental carbon 1.34% and organic carbon 9.46%

[d]Original data 20.56% as SiO_2

[e]Original data 1.3% ± 1.1% as SO_4^{2-}

[f]Original data 8.57% as Al_2O_3

sites on relatively open ground; all the other studies (Amato et al. 2009; Azarmi and Kumar 2016; Ramírez et al. 2019) took PM samples near active sites. This study detected significantly greater share of C (sum of elemental carbon and organic carbon), S, and Co, than the other four studies compared here (Amato et al. 2009; Azarmi and Kumar 2016; Jiang et al. 2018; Ramírez et al. 2019). The excessive amount of both C and S could be due to operations of machinery with diesel engines (Dorado et al. 2003; Ntziachristos et al. 2007; Robert et al. 2007; Thorpe and Harrison 2008) and proximity of the sampling location to the core of activities (20 m), because all other studies (Amato et al. 2009; Jiang et al. 2018; Ramírez et al. 2019) kept a distance up to 480 m from the site, except the one by Azarmi and Kumar (2016), who also suggested that PM_{10} mass concentration dwindled by half from the activity center to 80 m away. The mass fractions of Si and Al were lower than those in other studies (Amato et al. 2009; Azarmi and Kumar 2016; Jiang et al. 2018; Ramírez et al. 2019). Some detected carbon was also likely in the form of carbonate, such as $CaCO_3$, which is present in cement and similar materials.

When chemical composition differences between active sites and inactive sites are examined, Ca, Na, and Mg were generally found with greater mass fractions in the active ones; the demolition and construction activities present in active sites could contribute to elevated level of these elements (Dorado et al. 2003; Thorpe and Harrison 2008).

While the elemental analysis conducted here is convenient as it is accomplished with the same device as the image capture and allows the composition to be associated with particle morphology, any true safety- or regulatory-relevant examination of particle composition should include compound-specifying chemical analysis. That said, elemental analysis of solid particles like carbonates, oxides, phosphates, and nitrates can be examined on a worst-case basis to evaluate whether or not it is possible to exceed established exposure standards or recommendations. In this particular case, such exceedances are not possible. Such evaluation of any non-volatile hydrocarbons is not possible, however.

4.5 Implications for Image Analysis of Ambient Ultrafine Particles

The abundance of UFPs found throughout the impactor collection media regardless of stage necessitates further discussion as to its causes and implications for the interpretation of particle image analysis as a technique for studying ambient PM. This observation, in particular, has implications for traditional gravimetric analysis methods to correctly ascertain the level of exposure to UFPs.

There are three potential causes to this phenomenon: (1) UFPs existing as ambient UFPs were impacted randomly throughout impactor; (2) aggregated UFPs came apart before impact due to aerodynamic shear; and (3) aggregated UFPs came apart during impact.

How important each of these causes may be is likely dependent on the objectives of the particular investigation. Since, UFPs have been shown to be more toxic than larger particles (Kelly and Fussell 2012), it may be important to distinguish between ambient UFPs and UFPs that have aggregated or agglomerated into larger structures. Since the aerodynamic shear of collection in a cascade impactor exceeds the shear involved in human breathing, the relative proportion of UFPs may be only those existing as UFPs in the ambient environment. And, this method of collection and analysis will significantly overestimate the prevalence of these particles.

Although it is beyond the scope of this study, it may be possible to correct the UFP count, especially for those particles that apparently disaggregate during impact. This would involve an analysis of the spatial correlation of UFPs in relation to potential "parent" particles of larger sizes. Alternatively, a collection device with less energetic particle impacts may solve this potential measurement issue.

5 Conclusion

This study collected ambient PM samples from an active construction site at the Pennsylvania State University in four different occasions from September 2014 to September 2015 with a nine-stage cascade impactor and characterized the size distribution, shape distribution, and the elemental composition of the samples with TEMs and EDSs. 99.5% and 89.3% of the particles by count were finer than 1 µm and 0.1 µm, respectively. The mean PM count concentration was 16,232 particles/cm^3. The mean PM mass concentration was 167.2 µg/m^3, which is below the corresponding 8-h TWA PEL by OSHA, indicating no critical threat to occupational health. Both mean PM mass and number concentrations were consistent with values reported by studies focusing in outdoor activities and lower than those measured with indoor constructional or industrial activities. Regarding morphology, 72.2% of the particles had a circularity of between 0.9 and 1 and 74.0% of the particles had an aspect ratio of between 1:1 and 2:1; the correlation coefficient between circularity and aspect ratio was found to be − 0.5, indicating a minor negative correlation. Carbon, oxygen, silicon, sulfur, and calcium were the most prevalent elements found in the samples. The usage of machineries with diesel engines was considered a major contributor to sulfur, magnesium, and zinc. The demolition activities should elevate levels of silicon, aluminum, and cobalt.

Future work should focus on the automating physical and chemical analysis with to reduce the costs of such analyses. Researchers should consider the regular practice of

measuring the shape and chemical distributions of all PM samples especially in complex mixed environments to better facilitate comparison to laboratory toxicity data from the literature on manufactured particulates.

Acknowledgements This research has been supported by the National Institute of Occupational Safety and Health (NIOSH) through a John Hopkins Education and Research Center (ERC) for Occupational Safety and Health pilot grant (ERC – 2002170308). Any options, findings, conclusions or recommendations expressed in this material are those of the author(s) and do not necessarily reflect the views of NIOSH. The authors would also like to thank Miriam Freedman for her advice and suggestion during the sample collection and analysis phase.

Declarations

Conflict of Interest On behalf of all authors, the corresponding author states that there is no conflict of interest.

References

Allen JL, Oberdorster G, Morris-Schaffer K, Wong C, Klocke C, Sobolewski M, Conrad K, Mayer-Proschel M, Cory-Slechta DA (2017) Developmental neurotoxicity of inhaled ambient ultrafine particle air pollution: parallels with neuropathological and behavioral features of autism and other neurodevelopmental disorders. Neurotoxicology 59:140–154. https://doi.org/10.1016/j.neuro.2015.12.014

Amato F, Pandolfi M, Viana M, Querol X, Alastuey A, Moreno T (2009) Spatial and chemical patterns of PM10 in road dust deposited in urban environment. Atmos Environ 43:1650–1659. https://doi.org/10.1016/j.atmosenv.2008.12.009

American Conference of Governmental Industrial Hygienists (2005) TLVs and BEIs: based on the documentation of the threshold limit values for chemical substances and physical agents and biological exposure indices. Cincinnati, OH

Apple J, Vicente R, Yarberry A, Lohse N, Mills E, Jacobson A, Poppendieck D (2010) Characterization of particulate matter size distributions and indoor concentrations from kerosene and diesel lamps. Indoor Air 20:399–411. https://doi.org/10.1111/j.1600-0668.2010.00664.x

Asadi S, Hassan MM (2014) Worker exposure to ultrafine particles in asphalt laboratory. In: Kim RY (ed) Asphalt Pavements. CRC Press, pp 65–72. https://doi.org/10.1201/b17219

Ault AP, Peters TM, Sawvel EJ, Casuccio GS, Willis RD, Norris GA, Grassian VH (2012) Single-particle SEM-EDX analysis of iron-containing coarse particulate matter in an urban environment: sources and distribution of iron within Cleveland, Ohio. Environ Sci Technol 46:4331–4339. https://doi.org/10.1021/es204006k

Ault AP, Moffet RC, Baltrusaitis J, Collins DB, Ruppel MJ, Cuadra-Rodriguez LA, Zhao D, Guasco TL, Ebben CJ, Geiger FM, Bertram TH, Prather KA, Grassian VH (2013) Size-dependent changes in sea spray aerosol composition and properties with different seawater conditions. Environ Sci Technol 47:5603–5612. https://doi.org/10.1021/es400416g

Azarmi F, Kumar P (2016) Ambient exposure to coarse and fine particle emissions from building demolition. Atmos Environ 137:62–79. https://doi.org/10.1016/j.atmosenv.2016.04.029

Azarmi F, Kumar P, Mulheron M, Colaux JL, Jeynes C, Adhami S, Watts JF (2015) Physicochemical characteristics and occupational exposure to coarse, fine and ultrafine particles during building refurbishment activities. J Nanoparticle Res 17:1–19. https://doi.org/10.1007/s11051-015-3141-z

Bzdek BR, Pennington MR, Johnston MV (2012) Single particle chemical analysis of ambient ultrafine aerosol: a review. J Aerosol Sci 52:109–120. https://doi.org/10.1016/j.jaerosci.2012.05.001

Campos-Ramos A, Aragón-Piña A, Galindo-Estrada I, Querol X, Alastuey A (2009) Characterization of atmospheric aerosols by SEM in a rural area in the western part of México and its relation with different pollution sources. Atmos Environ 43:6159–6167. https://doi.org/10.1016/j.atmosenv.2009.09.004

Chrysikou LP, Samara CA (2009) Seasonal variation of the size distribution of urban particulate matter and associated organic pollutants in the ambient air. Atmos Environ 43:4557–4569. https://doi.org/10.1016/j.atmosenv.2009.06.033

Crilley LR, Lucarelli F, Bloss WJ, Harrison RM, Beddows DC, Calzolai G, Nava S, Valli G, Bernardoni V, Vecchi R (2017) Source apportionment of fine and coarse particles at a roadside and urban background site in London during the 2012 summer ClearfLo campaign. Environ Pollut 220:766–778. https://doi.org/10.1016/j.envpol.2016.06.002

D'Arcy JB, Dasch JM, Gundrum AB, Rivera JL, Johnson JH, Carlson DH, Sutherland JW (2016) Characterization of process air emissions in automotive production plants. J Occup Environ Hyg 13:9–18. https://doi.org/10.1080/15459624.2015.1076161

Debia M, Neesham-Grenon E, Mudaheranwa OC, Ragettli MS (2016) Diesel exhaust exposures in port workers. J Occup Environ Hyg 13:549–557. https://doi.org/10.1080/15459624.2016.1153802

Deshmukh DK, Deb MK, Mkoma SL (2013) Size distribution and seasonal variation of size-segregated particulate matter in the ambient air of Raipur city, India. Air Qual Atmos Health 6:259–276. https://doi.org/10.1007/s11869-011-0169-9

Dorado MP, Ballesteros E, Arnal JM, Gómez J, López FJ (2003) Exhaust emissions from a diesel engine fueled with transesterified waste olive oil. Fuel 82:1311–1315. https://doi.org/10.1016/S0016-2361(03)00034-6

Drewnick F, Dall'Osto M, Harrison R (2008) Characterization of aerosol particles from grass mowing by joint deployment of ToF-AMS and ATOFMS instruments. Atmos Environ 42:3006–3017. https://doi.org/10.1016/j.atmosenv.2007.12.047

Du Y, Xu X, Chu M, Guo Y, Wang J (2016) Air particulate matter and cardiovascular disease: the epidemiological, biomedical and clinical evidence. J Thorac Dis 8:E8–E19. https://doi.org/10.3978/j.issn.2072-1439.2015.11.37

Duclos JE (2015) Steidle building renewal project: technical report I. https://www.engr.psu.edu/ae/thesis/portfolios/2016/jid5237/PDF%27s/Tech_Report_I_jid5237.pdf. Accessed 15 Aug 2018

Falcon-Rodriguez CI, Osornio-Vargas AR, Sada-Ovalle I, Segura-Medina P (2016) Aeroparticles, composition, and lung diseases. Front Immunol 7:1–9. https://doi.org/10.3389/fimmu.2016.00003

Fent KW, Evans DE, Babik K, Striley C, Bertke S, Kerber S, Smith D, Horn GP (2018) Airborne contaminants during controlled residential fires. J Occup Environ Hyg 15:399–412. https://doi.org/10.1080/15459624.2018.1445260

Genga A, Siciliano T, Siciliano M, Aiello D, Tortorella C (2018) Individual particle SEM-EDS analysis of atmospheric aerosols in rural, urban, and industrial sites of Central Italy. Environ Monit Assess. https://doi.org/10.1007/s10661-018-6826-9

Hama SML, Cordell RL, Staelens J, Mooibroek D, Monks PS (2018) Chemical composition and source identification of PM10 in five North Western European cities. Atmos Res 214:135–149. https://doi.org/10.1016/j.atmosres.2018.07.014

HEI Review Panel on Ultrafine Particles (2013) Understanding the Health Effects of Ambient Ultrafine Particles. HEI Perspectives 3. Health Effects Institute, Boston, MA

Rasband WS, Image J. U. S. National Institutes of Health, Bethesda, Maryland, USA, pp 1997–2018. https://imagej.nih.gov/ij/

Järvelä M, Huvinen M, Viitanen AK, Kanerva T, Vanhala E, Uitti J, Koivisto AJ, Junttila S, Luukkonen R, Tuomi T (2016) Characterization of particle exposure in ferrochromium and stainless steel production. J Occup Environ Hyg 13:558–568. https://doi.org/10.1080/15459624.2016.1159687

Jiang N, Dong Z, Xu Y, Yu F, Yin S, Zhang R, Tang X (2018) Characterization of PM10 and PM2.5 Source Profiles of Fugitive Dust in Zhengzhou, China. Aerosol Air Qual Res 18:314–329. https://doi.org/10.4209/aaqr.2017.04.0132

Kelly FJ, Fussell JC (2012) Size, source and chemical composition as determinants of toxicity attributable to ambient particulate matter. Atmos Environ 60:504–526

Kittelson DB, Watts WF, Johnson JP (2004) Nanoparticle emissions on Minnesota highways. Atmos Environ 38:9–19. https://doi.org/10.1016/j.atmosenv.2003.09.037

Lavery AM, Waubant E, Casper TC et al (2018) Urban air quality and associations with pediatric multiple sclerosis. Ann Clin Transl Neurol 5:1146–1153. https://doi.org/10.1002/acn3.616

Lioy PJ, Weisel CP, Millette JR et al (2002) Characterization of the dust / smoke aerosol that settled east of the World Trade Center (WTC) in lower Manhattan after the collapse of the WTC 11 September 2001. Environ Health Perspect 110:703–714. https://doi.org/10.1289/ehp.02110703

Ntziachristos L, Ning Z, Geller MD, Sheesley RJ, Schauer JJ, Sioutas C (2007) Fine, ultrafine and nanoparticle trace element compositions near a major freeway with a high heavy-duty diesel fraction. Atmos Environ 41:5684–5696. https://doi.org/10.1016/j.atmosenv.2007.02.043

Olson E (2011) Particle shape factors and their use in image analysis - part 1: theory. J GXP Compliance 3:85–96

Ono-Ogasawara M, Serita F, Takaya M (2009) Distinguishing nanomaterial particles from background airborne particulate matter for quantitative exposure assessment. J Nanoparticle Res 11:1651–1659. https://doi.org/10.1007/s11051-009-9703-1

Penn State Office of Physical Plant (2018) Steidle building addition and renovation. https://opp.psu.edu/steidle-building-addition-and-renovation. Accessed 15 Feb 2019

Ramírez O, Sánchez AM, Campa D, Amato F, Moreno T, Silva LF, De JD, Sánchez de la Campa AM, Amato F, Moreno T, Silva LF, de la Rosa JD (2019) Physicochemical characterization and sources of the thoracic fraction of road dust in a Latin American megacity. Sci Total Environ 652:434–446. https://doi.org/10.1016/j.scitotenv.2018.10.214

Robert MA, Kleeman MJ, Jakober CA (2007) Size and composition distributions of particulate matter emissions: part 2 - heavy-duty diesel vehicles. J Air Waste Manag Assoc 57:1429–1438. https://doi.org/10.3155/1047-3289.57.12.1429

Scalf J, West P (2006) Introduction to nanoparticle characterization with AFM. Pac Nanotechnol Part 1:1–8. https://doi.org/10.1134/S0031918X10070021

Suhaimi NF, Jalaludin J (2015) Biomarker as a research tool in linking exposure to air particles and respiratory health. Biomed Res Int. https://doi.org/10.1155/2015/962853

The National Institute for Occupational Safety and Health (2011) Current intelligence bulletin 63: occupational exposure to titanium dioxide. DHHS (NIOSH) Publication No. 2011–160. U.S. Department of Labor, Washington DC

Thorpe A, Harrison RM (2008) Sources and properties of non-exhaust particulate matter from road traffic: a review. Sci Total Environ 400:270–282. https://doi.org/10.1016/j.scitotenv.2008.06.007

Occupational Safety and Health Administration (2018) Permisible Exposure Limits, Table Z-1. United States Department of Labor, Washington DC

Weiss F, Baloh P, Pfaller C, Can E, Kasper-giebl A, Wonaschütz A, Dimitrov M, Hofko B, Rechberger H, Grothe H, Cetintas EC, Kasper-giebl A, Wonaschütz A, Dimitrov M, Hofko B, Rechberger H, Grothe H (2018) Reducing paving emissions and workers' exposure using novel mastic asphalt mixtures. Build Environ 137:51–57. https://doi.org/10.1016/j.buildenv.2018.03.060

Yang Y, Mao P, Xu CL, Chen SW, Zhang JH, Wang ZP (2011) Distribution characteristics of nano-TiO2 aerosol in the workplace. Aerosol Air Qual Res 11:466–472. https://doi.org/10.4209/aaqr.2011.04.0038

Zhang Q, Gangupomu RH, Ramirez D, Zhu Y (2010) Measurement of ultrafine particles and other air pollutants emitted by cooking activities. Int J Environ Res Public Health 7:1744–1759. https://doi.org/10.3390/ijerph7041744